第 36 卷第 5 期
2017 年 10 月

红 外 与 毫 米 波 学 报
J. Infrared Millim. Waves

Vol. 36, No. 5
October, 2017

文章编号: 1001 - 9014(2017)05 - 0534 - 04

DOI:10.11972/j.issn.1001 - 9014.2017.05.004

Near-field imaging of the $LaAlO_3/SrTiO_3$ interfacial conductivity

CHENG Long[1,2], WANG Dong-Li[1,2], DAI Si-Yuan[3*], YAN Yue-Dong[1,2], FAN Xiao-Dong[1,2], WEI Lai-Ming[1,2], ZENG Chang-Gan[1,2*]

(1. Hefei National Laboratory for Physical Sciences at the Microscale, University of Science and Technology of China, Hefei 230026, China;
2. CAS Key Laboratory of Strongly-Coupled Quantum Matter Physics, and Department of Physics, University of Science and Technology of China, Hefei 230026, China;
3. Department of Physics, The University of California at San Diego, La Jolla, California 92093, USA)

Abstract: The $LaAlO_3/SrTiO_3$ heterointerface has been discovered to show two-dimensional interfacial conductivity and other intriguing emergent phenomena. Its interfacial conductivity was mainly characterized by electric methods previously. Here the authors present for the first time that scattering-type scanning near-field optical microscopy (s-SNOM) can be employed to spatially image the conductivity of the buried $LaAlO_3/SrTiO_3$ interface, providing a new means to study the physics of transition metal oxide heterointerface systems.

Key words: transition metal oxide heterointerface, $LaAlO_3/SrTiO_3$, interfacial conductivity, s-SNOM
PACS: 73.90. +f, 78.67.-n, 81.07.-b

$LaAlO_3/SrTiO_3$ 界面导电性的近场成像

成 龙[1,2], 王冬利[1,2], 戴思远[3*], 严跃冬[1,2], 范晓东[1,2], 魏来明[1,2], 曾长淦[1,2*]

(1. 中国科学技术大学 合肥微尺度物质科学国家实验室,安徽 合肥 230026;
2. 中国科学技术大学物理系 中科院强耦合量子材料物理重点实验室,安徽 合肥 230026;
3. 美国加州大学圣迭戈分校物理系, 美国 加州 拉荷亚 92093)

摘要:铝酸镧/钛酸锶($LaALO_3/SrTiO_3$)异质界面被发现具有二维导电性并呈现出其他一些有趣的呈展现象.而此前,$LaAlO_3/SrTiO_3$ 异质界面的导电性主要都是通过电学方法进行表征.这里作者首次提出利用散射式扫描近场光学显微镜(s-SNOM)对 $LaAlO_3/SrTiO_3$ 界面的导电性进行空间成像,这为研究过渡金属氧化物异质界面体系的物理现象提供了一个新的手段.

关 键 词:过渡金属氧化物异质界面;铝酸镧/钛酸锶;界面导电性;散射式扫描近场光学显微镜

中图分类号:O484.1;O484.4 + 1　　**文献标识码**:A

Introduction

The coupling of multiple degrees of freedom and the broken symmetries faciliate important fundamental phenomena and promising applications in transition metal oxide heterointerfaces[1-2]. As a prototypical example, two-dimensional (2D) electron system at the $LaAlO_3/SrTiO_3$ (LAO/STO) heterointerface exhibits remarkable properties including superconductivity[3-4], magnetism[5-6] and Rashba spin-orbit coupling[7-9] since the original discovery at 2004[10]. Useful device applications, such as photodetectors[11-12], gas sensor[13] and spintronic de-

Received date: 2017-02-10, **revised date**: 2017-07-07　　**收稿日期**:2017-02-10, **修回日期**:2017-07-07
Foundation items:Supported by National Basic Research Program of China (2014CB 921102), National Natural Science Foundation of China (11434009, 11374279, 11461161009), the Strategic Priority Research Program (B) of the Chinese Academy of Sciences (XDB01020000), the Fundamental Research Funds for the Central Universities (WK2030020027).
Biography:CHENG Long (1988-), male, Jiangsu, China. Doctoral candidate. Research fields focus on low-dimensional condensed matter physics. E-mail: dragoncl@mail.ustc.edu.cn
* **Corresponding author**:E-mail: siyuandai1991@gmail.com, cgzeng@ustc.edu.cn

vices[14-16], have also been reported. The intriguing physics and applications of LAO/STO interface mostly originate from the nature of 2D conductivity when the LAO thickness (d) exceeds a critical value ($d \geqslant 4$ unit cells (uc))[17]. This interfacial conductivity was typically characterized by the electric transport method[3-5, 8-10] which usually requires sophisticated electrode fabrication.

Scattering-type scanning near-field optical microscopy (s-SNOM), the antenna based nanoscope with optical resolution beyond the diffraction limit, may provide the alternative and more convenient method for local optical or electric property characterization[18-20]. Briefly, the scattered near-field signals detected by s-SNOM are closely related to permittivities of the materials[18, 21-22] and therefore can be used to discriminate between conducting and insulating behaviors considering their different dielectric properties. Utilizing this virtue, pioneering works have been demonstrated in nano-optical characterization of the carrier's spatial distribution of a silicon-based nanodevice[23] and the insulator-to-metal transition of VO_2 thin films[24]. However, direct detecting of transition metal oxide heterointerfaces via s-SNOM is rarely reported. Here we show that the non-invasive s-SNOM technique, can indeed be employed to effectively image the electric properties of the buried interface of LAO/STO heterostructure in real space.

1　Sample preparation

In the experiment, we fabricated the 3 μm by 3 μm LAO/STO periodic structure as shown in Fig. 1. LAO films were deposited on atomically flat STO substrates with TiO_2 termination by laser molecular beam epitaxy[9,12,25]. To obtain such structure, we first applied a standard UV lithography technique[26] to pattern the TiO_2-terminated STO substrate into the 3 μm by 3 μm periodic configuration (Fig. 1(a)); next, 3 nm thick amorphous LAO (a-LAO) films were deposited in an oxygen pressure of 2×10^{-2} mbar at room temperature (Fig. 1(b)); finally, after a lift-off step to remove the resist (Fig. 1(c)), LAO films were deposited at 700℃ with an oxygen pressure of 1×10^{-4} mbar and the thickness was monitored *in situ* by reflection high-energy electron diffraction (RHEED) intensity oscillations, the epitaxial LAO films were crystalline on the bare STO surface but amorphous on the a-LAO layer and the height difference between amorphous and crystalline LAO films should be kept constant (~ 3 nm, the thickness of a-LAO deposited in the prior step) (Fig. 1(d))[26]. This results in the alternating amorphous and crystalline LAO films on the TiO_2-terminated STO substrate, a typical scanning electron microscope (SEM) image of such structure is shown in Fig. 1(e), while Fig. 1(f) illustrates the s-SNOM measurement of such LAO/STO configuration.

We fabricated two kinds of representative LAO/STO samples with different thickness in terms of c-LAO films: the sample with 2uc c-LAO films is referred to as Sample A and that with 6uc c-LAO films is referred to as Sample B. Fig. 2(a) and 2(b) show the RHEED intensity oscillations of Sample A and Sample B during the c-LAO films growth, respectively. We also characterized the interfacial conductivity of a-LAO/STO, 2uc c-LAO/STO and 6uc c-LAO/STO. The former two is quite insulating with resistivity beyond the measurement limit, which is consistent with the results reported elsewhere[27], while the latter one is metallic as shown in Fig. 2(c). Therefore, for Sample A, the interfaces underneath a-LAO and c-LAO films are both insulating; while for Sample B, periodic insulating/conducting regions are formed at the interfaces underneath a-LAO/c-LAO films, which enables us to compare the s-SNOM signals of insulating a-LAO region with that of c-LAO region by subsequent s-SNOM detection, in order to determine the interfacial conductivity of c-LAO/STO.

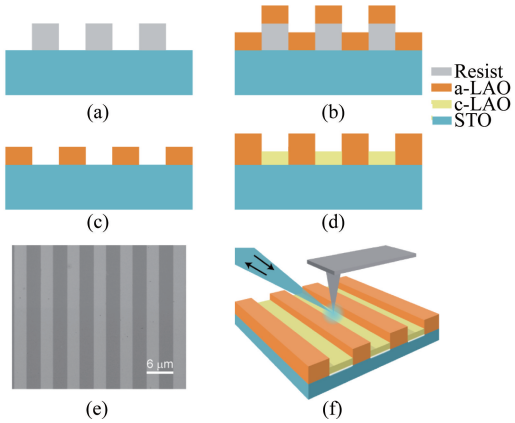

Fig. 1　(a ~ d) Illustration of the fabrication process: (a) lithography to produce periodic resist stripes on TiO_2-terminated STO substrate; (b) deposition of amorphous LAO film at room temperature; (c) a lift-off step to remove the resist; (d) deposition of LAO film at 700℃. (e) Scanning electron micrograph of the final LAO/STO structure. (f) Schematic of the LAO/STO configuration for s-SNOM measurement

图 1　(a ~ d) 样品制备流程示意图: (a) 光刻,使 TiO_2 为终止面的 STO 衬底上留有周期性的光刻胶条带; (b) 在室温下沉积非晶的 LAO 薄膜; (c) 去胶; (d) 在 700℃ 下沉积 LAO 薄膜. (e) 最终得到的 LAO/STO 结构的扫描电子显微图像. (f) LAO/STO 的 s-SNOM 测试图示

2　Measurements and results

The s-SNOM measurement was performed at 10.532 μm (corresponding to ~ 950 cm^{-1}) with the AFM tapping amplitude of 60 nm. In order to subtract the background signal, the scattered s-SNOM signal was demodulated at the 3rd harmonic of the tip-tapping frequency ~ 260 kHZ. Considering that the effective longitude probing depth amounts to tens of nanometers for s-SNOM measurement[28], and the LAO/STO interface is very close to the surface (~ 2.3 nm for 6uc LAO on STO), s-SNOM should be sensitive to the local conductivity property at the LAO/STO interfaces. Note that our nano-imaging experiments were performed at the frequency far away from the LAO/STO phonon resonances (Fig. 3)[29-30], therefore the s-SNOM signal can be predominantly related to the electronic properties of the sample. Simultaneously recorded s-SNOM images and AFM topography of Sample A and B are shown in Fig. 4. The a-

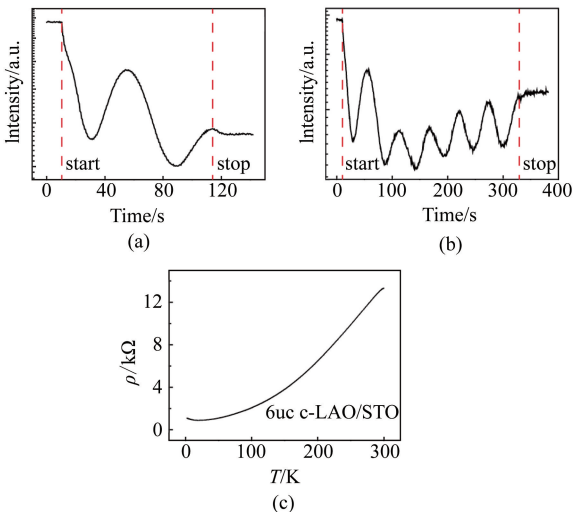

Fig. 2 (a,b) RHEED oscillations for the 2uc (a) and 6uc (b) c-LAO overlayers grown on the patterned STO substrates. (c) The resistivity of the 6uc c-LAO/STO interface as a function of the temperature

图 2 (a,b) 在 STO 衬底上外延生长 2uc (a) 和 6uc (b) 单晶 LAO 的 RHEED 振荡图. (c) 6uc c-LAO/STO 界面电阻率随温度的变化曲线

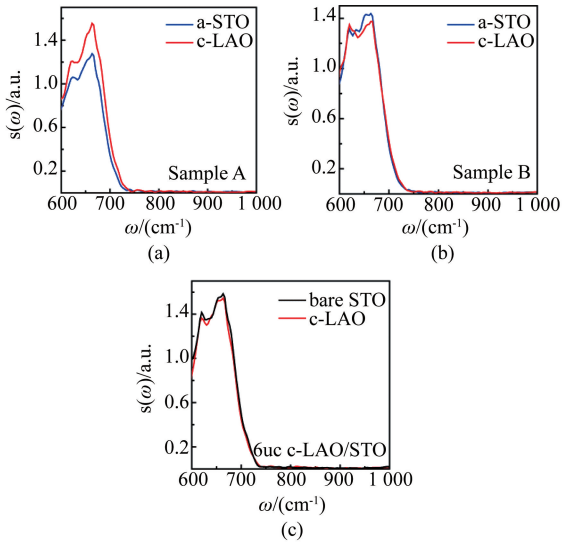

Fig. 3 (a,b) Nano-FTIR spectra of a-LAO (bule) and c-LAO (red) regions for Sample A (a) and Sample B (b). (c) Nano-FTIR spectra of c-LAO region (red) and bare STO surface (black) for an 6uc c-LAO/STO sample. All the spectra are normalized to that of gold

图 3 (a,b) 样品 A (a) 和样品 B (b) 的非晶 LAO(蓝色)和单晶 LAO(红色)区域的纳米分辨傅里叶变换红外谱. (c) 6uc c-LAO/STO 样品的单晶 LAO 区域(红色)和裸露的 STO 表面(黑色)的纳米分辨傅里叶变换红外谱. 所有的谱信号都归一化到金上

LAO regions (high) and c-LAO ones (low) can be discriminated due to the topographic difference (Figs. 4(a) and 4(b)). As shown in Fig. 4(c), the near-field amplitude of the a-LAO is slightly higher than that of the c-LAO in Sample A (2uc c-LAO). Since both the c-LAO/STO and a-LAO/STO interfaces are insulating in the case of Sample A, the difference in the near-field amplitude may originate from the tiny discrepancy in permittivities of the a-LAO and c-LAO films due to their different crystallinity and thickness[31-32]. Fig. 4(e) reveals the line profiles of AFM topography and near-field amplitude taken along the dashed line in Figs. 4(a) and 4(c) for Sample A, which indicates that the a-LAO region is ~3 nm higher than the c-LAO region as expected and the normalized near-field amplitude of the a-LAO region is about 10% higher than that of the c-LAO region.

Despite the small near-field signal difference in Sample A, more significant near-field contrast between a-LAO and c-LAO was observed in Sample B (6uc c-LAO, Fig. 4(d)). The detailed line profiles of AFM topography and near-field amplitude taken along the dashed line in Figs. 4(b) and 4(d) for Sample B shown in Fig. 4(f) display that the a-LAO is also ~3 nm higher than the c-LAO, similar as that in Sample A; while the normalized near-field amplitude of the a-LAO region is about 20% lower than that of the c-LAO region, in sharp contrast to that in Sample A. Since the near-field signal is positively related to the permittivity Re(ε)[18,21-22], the near-field signal contrast of Sample A (Fig. 4(b)), as well as the corresponding line profile (Fig. 4(e)), implies that the a-LAO/STO structure has a slightly larger permittivity than the 2uc c-LAO/STO structure, whereas for Sample B (Figs. 4(d) and 4(f)), the permittivity Re(ε) of a-LAO/STO structure is much smaller than that of 6uc c-LAO/STO structure. Considering that the 6uc c-LAO/STO interface is conducting in Sample B, in contrast to that in Sample A, the influence on the permittivity Re(ε) of the overlayer (a-LAO or c-LAO) may be overwhelmed by that of the interfacial conductivity. Therefore, one can qualitatively discriminate the interfacial conductivity of LAO/STO in real space by the near-field signal contrast.

3 Conclusion

In conclusion, we have demonstrated for the first time that the s-SNOM serves as a non-invasive optical technique to effectively probe the conductivity of the buried LAO/STO heterointerface with high spatial resolution in real space. This approach is expected to be powerful to image the local electric properties of buried interfaces of a spectrum of transition metal oxide heterostructures. Moreover, further developments of s-SNOM technique will enable the characterization of the heterointerfaces at cryogenic temperature and compatible with high magnetic field[33], which may provide further insight into the underlying physics.

References

[1] Chakhalian J, Millis A J, Rondinelli J. Whither the oxide interface [J]. *Nature Materials*, 2012, 11(2): 92-94.

[2] Hwang H Y, Iwasa Y, Kawasaki M, *et al.* Emergent phenomena at oxide interfaces[J]. *Nature Materials*, 2012, **11**(2):103-113.

[3] Reyren N, Thiel S, Caviglia A D, *et al.* Superconducting interfaces between insulating oxides[J]. *Science*, 2007, **317**(5842):1196-1199.

[4] Caviglia A D, Gariglio S, Reyren N, *et al.* Electric field control of the $LaAlO_3/SrTiO_3$ interface ground state [J]. *Nature*, 2008, **456**

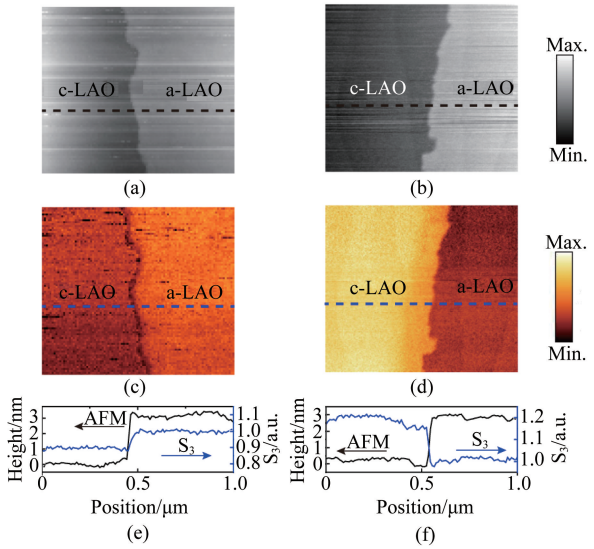

Fig. 4　(a, b) The AFM topographies at the boundaries between a-LAO and c-LAO regions for Sample A (a) and Sample B (b). (c, d) The corresponding infrared near-field amplitude imaging of Sample A (c) and Sample B (d). (e) The line profiles of AFM topography (black) and near-field amplitude (blue) taken along the corresponding dashed line in (a) and (c) for Sample A. (f) The line profiles of AFM topography (black) and near-field amplitude (blue) taken along the corresponding dashed line in (b) and (d) for Sample B. The near-field signals are normalized to that of a-LAO, respectively

图 4　(a, b) 样品 A (a)和样品 B (b)的非晶 LAO 和单晶 LAO 区域边界的 AFM 图像. (c, d) 样品 A (a)和样品 B (b)对应的红外近场强度图像. (e) 样品 A 沿着(a)和(c)中虚线的 AFM 形貌(黑色)和近场强度(蓝色)的轮廓曲线. (f) 样品 B 沿着(b)和(d)中虚线的 AFM 形貌(黑色)和近场强度(蓝色)的轮廓曲线. 近场信号分别归一化到非晶 LAO 上

(7222): 624 - 627.
[5] Brinkman A, Huijben M, Van Zalk M, *et al*. Magnetic effects at the interface between non-magnetic oxides[J]. *Nature Materials*, 2007, **6**(7): 493 - 496.
[6] Lee J S, Xie Y W, Sato H K, *et al*. Titanium d_{xy} ferromagnetism at the $LaAlO_3/SrTiO_3$ interface[J]. *Nature Materials*, 2013, **12**(8): 703 - 706.
[7] Shalom M B, Sachs M, Rakhmilevitch D, *et al*. Tuning spin-orbit coupling and superconductivity at the $SrTiO_3/LaAlO_3$ interface: a magnetotransport study[J]. *Physical Review Letters*, 2010, **104**(12): 126802.
[8] Caviglia A D, Gabay M, Gariglio S, *et al*. Tunable Rashba spin-orbit interaction at oxide interfaces[J]. *Physical Review Letters*, 2010, **104**(12): 126803.
[9] Liang H, Cheng L, Wei L, *et al*. Nonmonotonically tunable Rashba spin-orbit coupling by multiple-band filling control in $SrTiO_3$-based interfacial d-electron gases[J]. *Physical Review B*, 2015, **92**(7): 075309.
[10] Ohtomo A, Hwang H Y. A high-mobility electron gas at the $LaAlO_3/SrTiO_3$ heterointerface[J]. *Nature*, 2004, **427**(6973): 423 - 426.
[11] Irvin P, Ma Y, Bogorin D F, *et al*. Rewritable nanoscale oxide photodetector[J]. *Nature Photonics*, 2010, **4**(12): 849 - 852.
[12] Cheng L, Fan X, Wei L, *et al*. Photoconductivity of Graphene in Proximity to $LaAlO_3/SrTiO_3$ Heterostructures: Phenomenon and Photosensor Applications[J]. *Physical Review Applied*, 2016, **6**(1): 014005.
[13] Chan N Y, Zhao M, Huang J X, *et al*. Highly sensitive gas sensor by the $LaAlO_3/SrTiO_3$ heterostructure with Pd nanoparticle surface modulation[J]. *Advanced Materials*, 2014, **26**(34): 5962 - 5968.
[14] Swartz A G, Harashima S, Xie Y, *et al*. Spin-dependent transport across $Co/LaAlO_3/SrTiO_3$ heterojunctions[J]. *Applied Physics Letters*, 2014, **105**(3): 032406.
[15] Reyren N, Bibes M, Lesne E, *et al*. Gate-controlled spin injection at $LaAlO_3/SrTiO_3$ interfaces[J]. *Physical Review Letters*, 2012, **108**(18): 186802.
[16] Ngo T D N, Chang J W, Lee K, *et al*. Polarity-tunable magnetic tunnel junctions based on ferromagnetism at oxide heterointerfaces[J]. *Nature Communications*, 2015, **6**: 8035.
[17] Thiel S, Hammerl G, Schmehl A, *et al*. Tunable quasi-two-dimensional electron gases in oxide heterostructures[J]. *Science*, 2006, **313**(5795): 1942 - 1945.
[18] Atkin J M, Berweger S, Jones A C, *et al*. Nano-optical imaging and spectroscopy of order, phases, and domains in complex solids[J]. *Advances in Physics*, 2012, **61**(6): 745 - 842.
[19] Bonnell D A, Basov D N, Bode M, *et al*. Imaging physical phenomena with local probes: From electrons to photons[J]. *Reviews of Modern Physics*, 2012, **84**(3): 1343.
[20] Hillenbrand R, Taubner T, Keilmann F. Phonon-enhanced light-matter interaction at the nanometre scale[J]. *Nature*, 2002, **418**(6894): 159 - 162.
[21] Keilmann F, Hillenbrand R. Near-field microscopy by elastic light scattering from a tip[J]. *Philosophical Transactions of the Royal Society of London Series A-Mathematical Physical and Engineering Sciences*, 2004, **362**(1817): 787 - 805.
[22] YANG Z, WANG H, PENG X, *et al*. Recent progress in scanning probe microscope based super-resolution near-field fingerprint microscopy[J]. *J. Infrared Millim. Waves*(杨忠波, 王化斌, 彭晓昱, 等. 基于扫描探针显微镜的近场超空间分辨指纹光谱技术研究现状. **红外与毫米波学报**), 2016, **35**(1): 87 - 98.
[23] Huber A J, Keilmann F, Wittborn J, *et al*. Terahertz near-field nanoscopy of mobile carriers in single semiconductor nanodevices[J]. *Nano Letters*, 2008, **8**(11): 3766 - 3770.
[24] Qazilbash M M, Brehm M, Chae B G, *et al*. Mott transition in VO_2 revealed by infrared spectroscopy and nano-imaging[J]. *Science*, 2007, **318**(5857): 1750 - 1753.
[25] Liang H, Cheng L, Zhai X, *et al*. Giant photovoltaic effects driven by residual polar field within unit-cell-scale $LaAlO_3$ films on $SrTiO_3$[J]. *Scientific Reports*, 2013, **3**: 1975.
[26] Schneider C W, Thiel S, Hammerl G, *et al*. Microlithography of electron gases formed at interfaces in oxide heterostructures[J]. *Applied Physics Letters*, 2006, **89**(12): 122101.
[27] Chen Y, Pryds N, Kleibeuker J E, *et al*. Metallic and insulating interfaces of amorphous $SrTiO_3$-based oxide heterostructures[J]. *Nano Letters*, 2011, **11**(9): 3774 - 3778.
[28] Kawata S. Near-Field Optics and Surface Plasmon Polaritons[M]. Springer Science & Business Media, 2001.
[29] Perry C H, Fertel J H, McNelly T F. Temperature dependence of the Raman spectrum of $SrTiO_3$ and $KTaO_3$[J]. *The Journal of Chemical Physics*, 1967, **47**(5): 1619 - 1625.
[30] Akimov I A, Sirenko A A, Clark A M, *et al*. Electric-field-induced soft-mode hardening in $SrTiO_3$ films[J]. *Physical Review Letters*, 2000, **84**(20): 4625.
[31] Busani T, Devine R A B. Molecular volume and electronic and vibrational polarizibilities for amorphous $LaAlO_3$[J]. *Journal of Applied Physics*, 2004, **96**(11): 6642 - 6647.
[32] Yan L, Kong L B, Ong C K. The effect of ultra-thin Al_2O_3 layers on the dielectric properties of $LaAlO_3$ thin film on silicon[J]. *Semiconductor Science and Technology*, 2004, **19**(7): 935.
[33] Yang H U, Hebestreit E, Josberger E E, *et al*. A cryogenic scattering-type scanning near-field optical microscope[J]. *Review of Scientific Instruments*, 2013, **84**(2): 023701.